

Two-center effects in electron emission in ${}^3\text{He}^{2+}$ -He and H^+ -He collisions at intermediate energies

G. C. Bernardi, S. Suárez, P. D. Fainstein, C. R. Garibotti, W. Meckbach, and P. Focke
*Comisión Nacional de Energía Atómica, Centro Atómico Bariloche,
 8400 San Carlos de Bariloche, Argentina*

(Received 8 June 1989)

We present measurements of doubly differential cross sections (DDCS) with respect to energy and angle for electron emission produced when 100- and 50-keV/u ${}^3\text{He}^{2+}$ and H^+ collide with He. An electron spectrometer designed for this purpose enables us to measure electron distributions which, even at small emission angles, do not present appreciable deformations of the measured distributions by extended gas target effects. Using the ratio of the emissions obtained with ${}^3\text{He}^{2+}$ and H^+ , we study the dependence of the DDCS on the projectile charge. We confirm a saturation of this emission ratio that increases with increasing angle. Furthermore, we report a sudden enhancement of the emission ratio that is found at and above the electron capture to the continuum peak. These observations are in basic but not quantitative agreement with calculations performed using a model that incorporates the continuum distorted wave and eikonal initial state and that approximately accounts for a two-center interaction of the active electron.

I. INTRODUCTION

The single ionization of atomic targets in ion-atom collisions has been the subject of extensive experimental and theoretical research. Earlier efforts had been directed towards the theoretical and experimental analysis of total ionization cross sections (σ_I) with reference to their dependence on the energy (E_p) and charge (q) of the projectile.¹ Perturbative first-order theories, such as the binary encounter approximation (BEA) and the first-order Born approximation (FBA), predict that σ_I is proportional to the square of the projectile charge q^2 . These approximations, however, are only valid at large energies. In fact Niels Bohr² has shown that, if the velocity of the projectile (v_p) is of the order or smaller than the charge q (in atomic units) or the initial orbital velocity of the active target electron, the charge dependence of σ_I tends to saturate. This "saturation effect" has been further investigated by Gillespie,³ who introduced a relevant dynamical variable, the so called "reduced projectile velocity" $v_R = v_p/q^{1/2}$, equivalent to a "reduced energy per amu" $E_R = (E_p/A)/q$, where A is the atomic weight. He showed that the ratio $\sigma_I/q^2\sigma_{\text{FBA}}$ can be represented as a function of this variable in a unified manner for ionic projectiles of different charges q . This suggests that the deviation of the cross section from the q^2 dependence can be attained not only with fast highly charged ions, but also with projectiles of lower charge at intermediate energies. Recent calculations, that employ the Glauber approximation and the Schwinger variational principle⁴⁻⁶ deviate from the FBA for $v_p \lesssim q$, giving a reasonable description of the saturation of total ionization and excitation cross sections.

The study of the total cross section alone cannot give detailed insight into the mechanisms governing electron production in ion-atom collisions. More information is

furnished by measurements of double differential distributions $Q(E_e, \theta)$, as a function of the electron energy E_e and angle of emission θ relative to the direction of the projectile path. In Fig. 1 we show such a distribution as a function of the electron velocity v_e , for H^+ +He collision at 170 keV.⁷ The measured signal Q has been divided by v_e^3 in order to account for the increase of the experimental resolution with the third power of the electron velocity.⁸ We observe the typical electron capture to the continuum (ECC) cusp, centered at the projectile velocity $v_e = v_p$, and the initial slope of the overwhelming direct ionization (DI) peak which is centered at the origin $v_e = 0$.

Perturbative one-center theories led to the description of the final state of ECC and DI electrons in terms of Coulomb waves, centered at the projectile and the target,

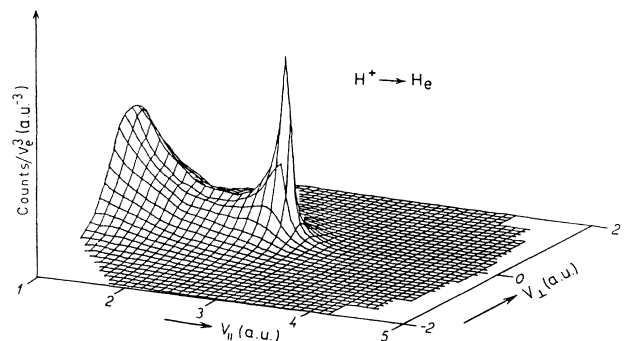


FIG. 1. Three-dimensional representation of a double differential distribution of electrons emitted when 170-keV H^+ interact with He, represented as a function of the longitudinal v_{\parallel} and transverse v_{\perp} components of the electron velocity v_e . The measured signal has been divided by v_e^3 . From Ref. 7.

respectively.^{9,10} However, during the collision, the active electron is subjected to the interaction with both centers: the ionic projectile and the core of the target. Therefore, its final state must be described as a quasimolecular continuum state.¹¹ This two-center effect is the physical cause of the well-known longitudinal asymmetry, that is, an enhancement for $v_e < v_p$, of the ECC peak.¹² At lower velocities the electron is subjected to the simultaneous attraction of both the projectile and target on a comparable footing, tending to be confined in the saddle potential between these two centers.¹³ This mechanism leads to a broad longitudinal ridge-shaped enhancement, clearly distinguished in Fig. 1. This figure replaces Fig. 2 of Ref. 13, where a sharp knife-edge-shaped configuration, caused by an experimental artifact (see Sec. II of this paper and Ref. 7), was superimposed.

Double differential angular distributions, measured in this laboratory at different electron energies, for 50–200-keV H^+ interacting with He-gas target, have been presented by us, together with previous experimental information.¹⁴ On the other hand such distributions, which put into quantitative evidence the above mentioned ridge shaped structure, have been compared with different theoretical approaches that approximately account for the collisional two-center Coulomb interaction of the emitted electron.¹⁵

This “two-center electron emission” (TCEE) has subsequently been studied using heavier ions, by Stolterfoht *et al.*,¹⁶ who reported, in accordance with the appearance of the above-mentioned ridge, an increase of the electron emission in the forward direction in $Mo^{40+} + He$ collisions at 25 MeV/u. An observed decrease in the backward direction was also attributed to TCEE. Similar measurements with 5-MeV/u C^{6+} , O^{8+} , and Ne^{10+} on He were performed by Platten *et al.*¹⁷ and discussed by Fainstein *et al.*¹⁸ in terms of the “continuum-distorted-wave–eikonal-initial-state” (CDW EIS) model.¹⁹ The cited measurements cover only electron energies below the electron equivalent ion energy (E_{eq}), that is, the energy of the ECC peak.

The aim of the present work is to explore the projectile charge dependence of double differential distributions of electrons produced in the collisional ionization of He gas by ions of low charge at intermediate energies. We used H^+ and ${}^3He^{2+}$ with reduced energies between 0.025 and 0.1 (MeV/u)/ q . Deviations from first-order single Coulomb center theoretical interpretations are expected to be relevant at these energies. Our measurements, which cover an expanded range of electron energies beyond the ECC peak energy (E_{eq}), confirm the increase of saturation with increasing emission angle θ . Furthermore we find at $v_e = v_p$ a remarkable stepwise increase of the ratio of the emissions induced by ${}^3He^{2+}$ and H^+ . Both properties are found to be in qualitative agreement with CDW EIS calculations. A preliminary account of our findings has been presented in Ref. 20.

II. EQUIPMENT AND MEASUREMENTS

The electron distributions $Q(E_e, \theta)$ (double differential with respect to energy E_e and emission angle θ) have been measured with our newly designed electron spec-

trometer shown in Fig. 2. A detailed description of this equipment has been given in Ref. 7. Here we only present an account of its basic properties and those specific features that are relevant to the reliability of the experimental results. Because of its known distinguished focusing properties, we choose the coaxial cylindrical configuration.²¹ The incident ion beam is collimated to a 0.5 mm diameter and an angular spread of less than 0.1° . Beam intensities were of the order of 1.5×10^{-8} A for H^+ and 2×10^{-10} A for ${}^3He^{2+}$. The target, provided by an atomic gas stream emerging from the tip of a hypodermic needle with a 0.25 mm bore, is localized at the intersection of the ion beam, the spectrometer axis, and a third axis around which the spectrometer can be turned for measurement at different angles θ . The electron beam path through the spectrometer is such that an image of the target is formed on its axis, where a 0.5-mm-diam orifice O_1 defines the energy resolution ($\Delta E_e/E_e = 0.4\%$). The angle θ of measurement, as well as the half angle θ_0 of the accepted electron cone, are defined by O_1 and a second orifice O_2 situated at the spectrometer exit or, more precisely, by the virtual image of O_2 centered on a prolongation of the axis of the electron beam that enters the spectrometer before being deflected. The basic advantage of this configuration is that the ion beam is never intercepted by the frame of O_2 . This facilitates measurement at any angle θ , including small angles. There is a choice of six angular resolutions, between $\theta_0 = 0.25^\circ$ and 2.5° . For the present measurements we use $\theta_0 = 2^\circ$.

An outstanding feature of this spectrometer is the low “target out” background, caused by slit scattering and eventual rest gas counts. It amounts to less than 1.5%, even in regions where the signal $Q(E_e, \theta)$ is low (see also Fig. 3 of Ref. 7). From Fig. 4 of Ref. 7 one can observe that our spectrometer is able to register electron spectra down to energies below 3 eV. This is a consequence of a careful internal and external alignment of the spectrometer, a correct localization of the target, as well as elimination of factors which may distort the electron paths, such as stray magnetic fields and spurious electric fields produced by local surface charges. These precautions also allow for the symmetry of the distributions with respect

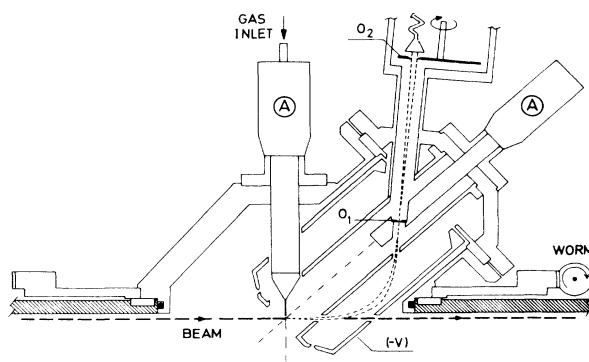


FIG. 2. Coaxial cylindrical electron spectrometer for measurement of electron distributions as a function of energy E_e and emission angle θ . For details, see text and Ref. 7.

to measurements at "positive" and "negative" angles θ , which were found to be within 5% for angles between 0° and 15° and 10% elsewhere. Furthermore, we were able to reduce those deformations of the measured distributions due to extended gas target effects to such an extent that they were almost comprised within random fluctuations of the registered electron emission. Two distinct causes had to be accounted for an extended target: (i) an overall distributed gas pressure in the scattering chamber and (ii) an extension of the atomic gas stream emerging from the needle tube. A quantitative study of these two effects can be found in Ref. 7. They were minimized by (i) directing the gas stream into the throat of a 1500 l/s pumping system and (ii) placing the needle tip at a dis-

tance of only 0.1 mm from the edge of the ion beam, that is about 0.3 mm from its axis. Even though many estimates of the effects produced by extended targets can be found in the literature, to our knowledge there is no quantitative study of the consequent deformations of double differential distributions, such as those contained in Figs. 2(a) and 2(b) of our Ref. 7. These effects are particularly troublesome in the range of small angles, not covered in most up-to-date measurements. For instance in Fig. 2 of our Ref. 13, a sharp longitudinal crest appeared as an artifact superimposed on top of the measured distributions. In our previous electron analyzer we tried to pump the target gas with a separate system.⁸ However, this procedure implied the introduction of a large vacuum impedance.

In Figs. 3(a) and 3(b) we present a series of double differential electron spectra for 100-keV/u H^+ and ${}^3\text{He}^{2+}$ incident on He, measured at angles θ in steps of 10° between 0° and 90° and between 0° and 70° , respectively. Equivalent spectra were measured at 50 keV/u, but due to small count rates, they could, for ${}^3\text{He}^{2+}$, be measured only up to 50° . Special care has been taken with respect to the mutual consistency of the measured spectra. As it took many hours to obtain a set of spectra as those seen in Fig. 3, long-term fluctuations, particularly those related to the effective gas target thickness, were difficult to control. However, we verified the reproducibility, within statistical errors, of immediate repetitions of measurement of one energy spectrum and angular distributions. Then an internal consistency of our data within 10% was achieved by normalizing all the individual energy spectra to one angular distribution taken at a specified energy. These particular angular distributions, used for the normalization of the $\text{H}^+ + \text{He}$ and ${}^3\text{He}^{2+} + \text{He}$ data, are seen in Fig. 4.

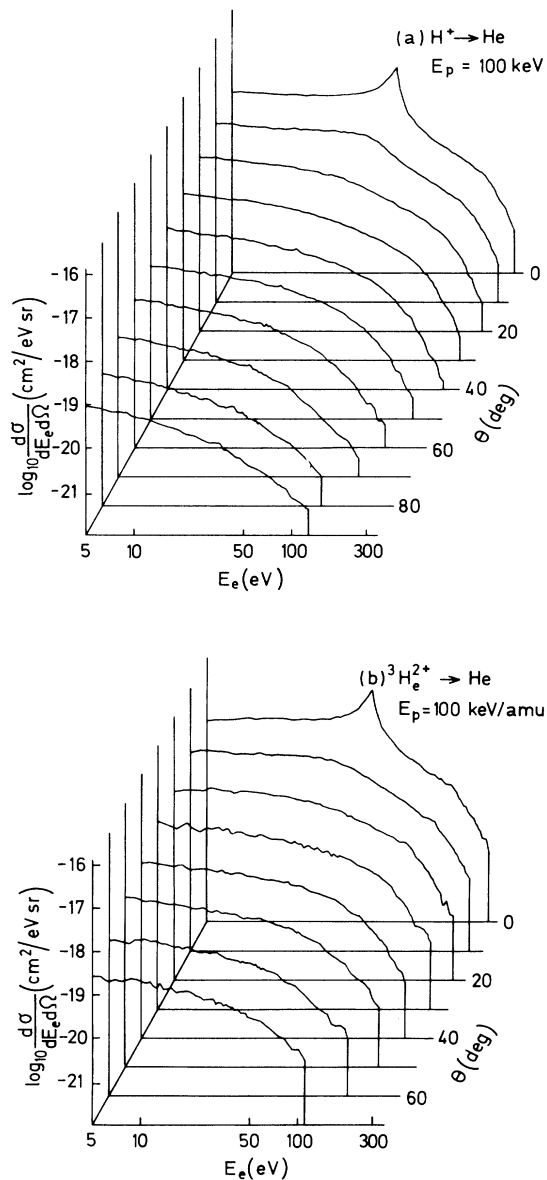


FIG. 3. Double differential electron spectra measured as a function of emitted electron energy E_e at angles θ in steps of 10° with (a) H^+ and (b) ${}^3\text{He}^{2+}$ of 100 keV/u.

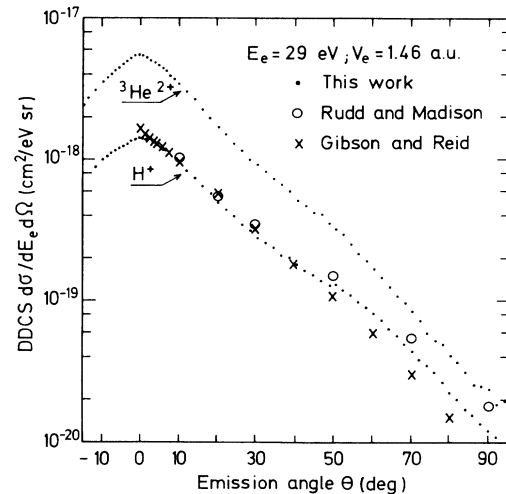


FIG. 4. Absolute double differential angular distributions of electrons emitted with an energy of $E_e = 29 \text{ eV}$ when 100-keV/u H^+ and ${}^3\text{He}^{2+}$ interact with He. These distributions have been used for internal consistency of the data contained in Fig. 3 and also are compared with (\circ) Rudd and Madison (Ref. 22) and (\times) Gibson and Reid (Ref. 23).

In order to be able to perform a quantitative comparison of double differential electron distributions, produced by projectiles of different mass but equal velocity, we adjusted the accelerator voltage in such a way that the sharp ECC peak tops were superimposed on the electron energy scale. This procedure was justified because in the first place there is no doubt that cusp peaks are localized at E_{eq} , and secondly this did not imply a shift beyond the error limits of $\pm 1.5\%$ of the calibration of our accelerator.

With respect to the possible presence of projectiles that have captured electrons in the beam transport between the sorting magnet of the accelerator and the target, using measured pressures and known cross sections for charge exchange, we estimated upper limits of 2.5% and 0.6% of H^0 projectiles in the incident proton beam, and 3% and 2% of He^+ projectiles, and 1% and 0.4% of He^0 projectiles in the incident ${}^3He^{2+}$ beam at 50 and 100 keV/u, respectively. Systematic errors in our measurements produced by ionization of these contaminants would be most notable at low electron-projectile velocities. In an independent-experiment we verified that the yield of the electron loss to the continuum (ELC) process from H^0 is 1.7 times that for electron capture to the continuum (ECC) of H^+ at 50 keV, and 2.6 times at 100 keV. Consequently we can estimate that for H^+ projectiles contributions of ELC from H^0 to our measured data were of the order of 4% and 1.5% or less. For ${}^3He^{2+}$ projectiles the relative ELC contribution is even smaller. Furthermore, we varied the gas pressure, within limits of 1:10, in the region of beam transport to the target without being able to observe any change in the shape of the measured electron spectra obtained with incident H^+ and ${}^3He^{2+}$.

Besides single-target ionization, other additional processes, such as double ionization and transfer ionization, may contribute to the measured distributions. In Table I we show percentages of the total electron emission due to these processes, estimated from data in Ref. 1. We see that mainly transfer ionization, which is particularly large for ${}^3He^{2+}$ at 50 keV/u, can introduce an uncertainty in our data. Coincidence measurements of double

TABLE I. Contribution (in percent) for single ionization (SI), double ionization (DI), and transfer ionization (TI) in the total electron production from data in Ref. 1.

	$E_p = 50$ keV/u		$E_p = 100$ keV/u	
	H^+ ^a	${}^3He^{2+}$	H^+	${}^3He^{2+}$
SI	95.4	64.1	96.9	84.3
DI	2.5	3.8	2.2	4.9
TI	2.1	32.1	0.9	10.8

^aExtrapolated values.

differential distributions would serve to establish these contributions. However, due to low count rates at larger angles, particularly for the low intensity ${}^3He^{2+}$ beams, such measurements were not feasible in the context of the present work.

III. RESULTS AND DISCUSSION

In Figs. 5(a) and 5(b) we present double differential electron distributions as obtained with 100-keV/u H^+ and ${}^3He^{2+}$ projectiles as a function of E_e . In order to avoid excessive complication of this figure, we do this only for selected angles θ of emission. For H^+ [Fig. 5(a)] we compare with previous measurements of Rudd and Madison²² and Gibson and Reid.²³ We did not include data from Refs. 24 and 25, which are in good agreement with Rudd and Madison.

We transform our distributions to absolute DDCS by normalizing the numerically integrated total cross section for 100 keV H^+ with the value recommended in a compilation by Rudd *et al.*²⁶ The evaluation of the integral

$$\sigma_I = 2\pi \int_0^\infty dE_e \int_0^\pi \sin\theta d\theta \frac{d\sigma}{dE_e d\Omega}$$

implies some premises. Firstly low energy electrons, not included in our data, are introduced considering $d\sigma/dE_e d\Omega = v_e (d\sigma/dv_e)$ constant below $E_e = 5$ eV. This is based on the assumption that close to $v_e = 0$ the post-collisional electron wave function is dominated by a Coulomb wave, and consequently

TABLE II. Total ionization cross sections σ_I (cm^2). Values in square brackets are exponents of ten. Our integrated data have been normalized for 100-keV H^+ to the value recommended by Rudd *et al.* (Ref. 26). Also included are data from Refs. 1 and 28, as well as cross sections calculated using the CDW EIS approximation and the classical trajectory Monte Carlo (Ref. 29) method.

	$E_p = 50$ keV/u		$E_p = 100$ keV/u	
	H^+	${}^3He^{2+}$	H^+	${}^3He^{2+}$
Integrated DDCS (this work)	8.50[−17]		9.26[−17]	2.67[−16]
Compilation (Ref. 26) Rudd <i>et al.</i>	7.89[−17]		9.26[−17]	
Shah and Gilbody (Ref. 1)	7.33[−17]	1.12[−16]	8.70[−17]	2.19[−16]
Puckett <i>et al.</i> (Ref. 28)		1.55[−16]		2.47[−16]
CDW EIS	8.34[−17]	1.20[−16]	9.99[−17]	2.57[−16]
CTMC	9.07[−17]	1.11[−16]	1.07[−16]	2.80[−16]

$d\sigma/dv_e = d\sigma/v_e^2 dv_e d\Omega \sim 1/v_e$. Secondly, our measurements did not include angles $\theta > 90^\circ$. In that range we took advantage of previous evidence²⁷ which indicates that the single differential cross section, resulting from an integration over E_e , is also approximately constant. In Table II we see that the described normalization for 100-keV H^+ leads to a consistency in the total cross sections σ_I , within known error limits ($\approx 15\%$), with σ_I values quoted for 50-keV H^+ and 100-keV/u ${}^3\text{He}^{2+}$ from Refs. 1 and 28.

We observe in Fig. 5(a) that our data fall between those of Rudd and Madison²² and Gibson and Reid²³ for $\theta=90^\circ$ and 50° . A better agreement of our DDCS with those of Ref. 22, as compared to Ref. 23, is observed for $\theta=10^\circ$. For $\theta=0^\circ$ the only comparable information is from Ref. 23. We find that these data are larger than ours, particularly in the range below the ECC peak top. We have also included the DDCS of Refs. 22 and 23 in Fig. 4, where we present a double differential angular distribution, taken at $E_e=29$ eV with 100-keV/u H^+ and ${}^3\text{He}^{2+}$. Good agreement is observed at the lower angles. Above $\theta=40^\circ$ our DDCS again fall between those of Rudd and Madison²² and Gibson and Reid.²³ For the ${}^3\text{He}^{2+}$ data in Figs. 5(b) and 4 there is no experimental evidence to compare with. A table, containing complete information of our measured DDCS, can be furnished upon request.

We also present in Figs. 5(a) and 5(b) a comparison of our results with calculations based on the CDW EIS approximation.¹⁸ This model proposes an entry channel where the target bound state is multiplied by an eikonal phase that provides the distortion associated with the electron-projectile interaction. This distorted initial-state wave function is normalized and satisfies the correct asymptotic conditions. For the He target the initial active-electron bound state is approximated by a Roothaan-Hartree-Fock wave function and the other electron is considered frozen during the collision. In the final state the electron is described by a wave function written as a product of two continuum states, one centered on the projectile and the other centered on the target. This proposed final state also satisfies the correct asymptotic conditions. In this way the initial and final states introduce two-center effects by considering the distortion of the electronic state due to the presence of both, the target and the projectile Coulombic potentials.

In Fig. 5(a), at energies smaller than E_{eq} and for $\theta=0^\circ$ and 10° , the theoretical DDCS stay below the experimental ones by a factor of about 3, whereas for $\theta > 30^\circ$ they tend to be larger. This means that the CDW EIS model does show, but underestimates, the enhancement or ridge shaped structure which, in this region, was found to be characteristic for a two center interaction of the emitted electron.¹³⁻¹⁵ At the larger emission angles and energies the theoretical DDCS stay below the experimental ones. A similar, even more pronounced, behavior is seen in Fig. 5(b) for the case of ${}^3\text{He}^{2+}$ projectiles. Further and more complete evidence concerning comparison of experimental double differential electron distributions measured in this laboratory, with existing experimental information and different theoretical approaches, can be found in

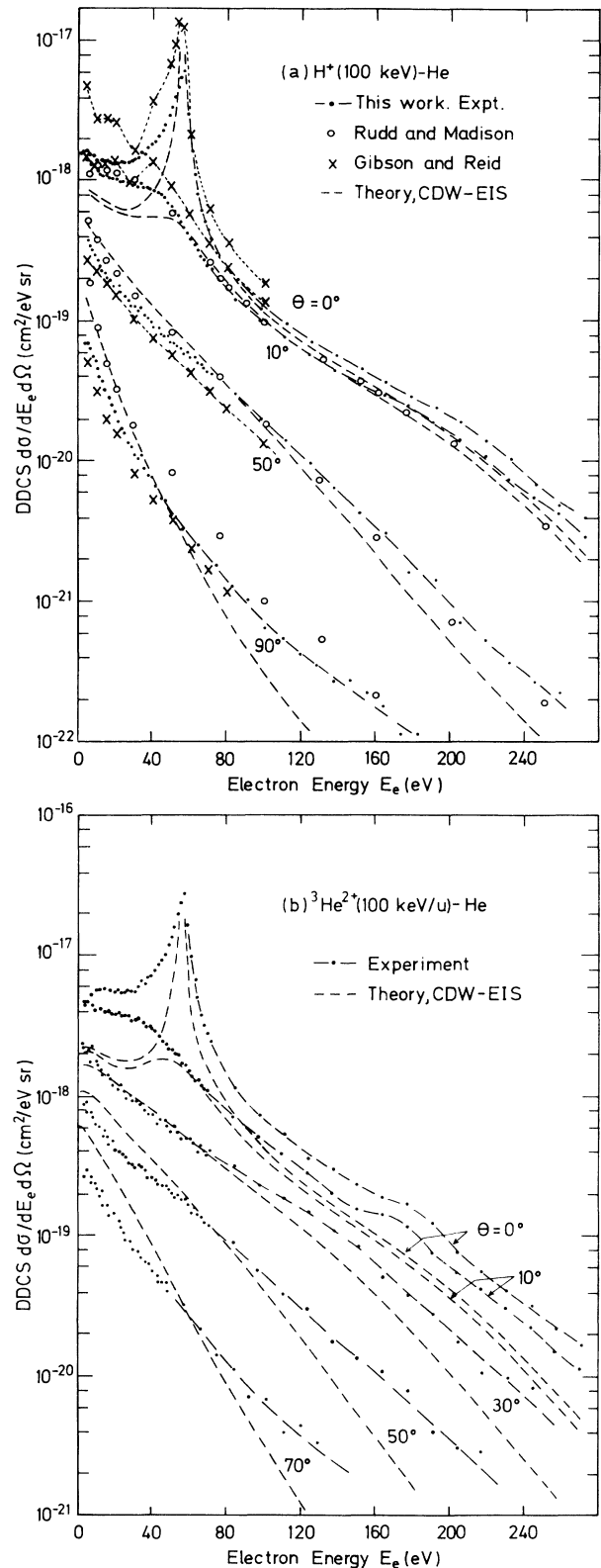


FIG. 5. Absolute double differential energy distributions of electrons emitted at fixed emission angles θ when (a) H^+ and (b) ${}^3\text{He}^{2+}$ of 100 keV/u interact with He. Comparison is shown with (\circ) Rudd and Madison (Ref. 22), (\times) Gibson and Reid (Ref. 23), and (---) the CDW EIS theory.

Refs. 14 and 15.

We also evaluated single differential angular distributions (SDAD) from our data, with the premises already announced above with relation to the normalization to the total cross sections. We note in Figs. 6(a) and 6(b) that at a given energy the SDAD for ${}^3\text{He}^{2+}$ is steeper than that for H^+ . This can be interpreted as a consequence of the focusing properties of the increased projectile charge.³⁰ We also show results from the CDW EIS and “classical trajectory Monte Carlo” approximations.²⁹ As already observed for the DDCS, the CDW EIS method underestimates the emission at small angles and low energies.

We finally look for the dependence of the measured double differential electron emission on the projectile charge q , by dividing those obtained with doubly charged ${}^3\text{He}^{2+}$ through those obtained with single charged H^+ . The resulting double differential ratios $R(E_e, \theta)$ are shown in Figs. 7(a) and 7(b). Due to the uncertainties in the normalization of the electron energy spectra, measured with incident ${}^3\text{He}^{2+}$ and H^+ , respectively (see Sec. II), an error of $\pm 10\%$ must be considered in the ratio R for each angle of emission.

In Fig. 7 we observe strikingly different behaviors for $R(E_e, \theta)$ on both sides of the electron equivalent ion energy E_{eq} , that is, the energy of the ECC peak.

(i) In the lower electron energy range, $E_e < E_{eq}$, only a weak dependence of the ratio R on E_e is observed. In this range $R \leq q_{\text{He}}^2 = 4$ at all angles. The ratio R tends to decrease with increasing θ . This means that there is, in accordance with theoretical predictions and the findings recorded for the case of heavier ions in Refs. 16 and 18, a saturation which becomes more accentuated at larger emission angles θ . One concludes that, as the saddle potential between the ion and the residual target is more pronounced in the case of the projectile of higher charge (${}^3\text{He}^{2+}$), the ridge-shaped structure found along the forward direction also becomes more pronounced compared with that resulting with the less charged projectile (H^+). This enhancement of the longitudinal shoulder with increasing projectile charge, already evident from a comparison of the double differential angular distributions of Figs. 4(a) and 4(b), is an additional clear indication of the importance of the two-Coulomb-center interaction of the emitted electrons.

(ii) A most remarkable feature of the ratio $R(E_e, \theta)$ in Figs. 7(a) and 7(b) is the upwards step in the forward direction. It seems as if the projectile of higher charge is capable of throwing more electrons into the velocity range above v_p . For $\theta = 0^\circ$ this abrupt change is strongest and appears just at E_{eq} , the energy of the ECC peak top. This enhancement of R up to about 6 is followed, in the case of Fig. 7(b) (100 keV/u), by a gradual decrease which is not seen in Fig. 7(a) (50 keV/u) within the covered electron energy range.

An increase, close to E_{eq} , of the electron emission ratio can also be deduced from double differential distributions of Toburen and Wilson,³¹ as shown in Fig. 8, where we present a dependence of $R(E_e, \theta)$ as it was extracted from electron energy spectra contained in their Fig. 1, measured at $\theta = 30^\circ$ with 75-keV/u He^{2+} and 70-keV H^+ on

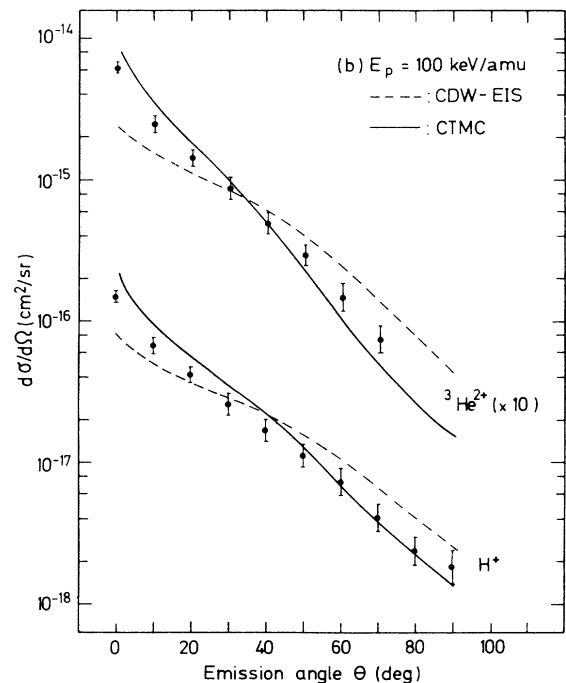
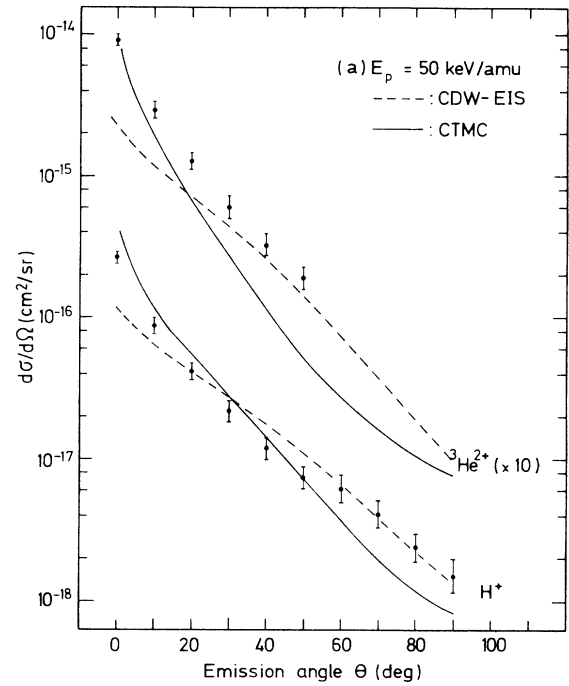


FIG. 6. Single differential cross sections as a function of the emission angle θ for (a) 50-keV/u and (b) 100-keV/u H^+ and ${}^3\text{He}^{2+}$ on He. Comparison is shown with the CDW EIS approximation (---) and the classical trajectory Monte Carlo method (—).

Ar, and angular distributions shown in their Fig. 5. A behavior, similar to our R dependence for $\theta=30^\circ$ in Fig. 7(b), can be seen. The authors mention a minor lack of consistency of these data, due to the fact that the H^+ measurements are made by a different author³² and are obtained at a slightly different energy. However, since the variation of R with E_e is slow for $\theta=30^\circ$, this does not seriously affect the dependence shown in Fig. 8.

For $\theta=0^\circ$ and close to $E_e=E_{\text{eq}}$ the above mentioned step in $R(E_e, \theta)$ means an enhancement of the high-energy tail of the ECC peak for the projectile of higher charge. This can be clearly distinguished in Fig. 9 where we show longitudinal peaks as measured with H^+ and ${}^3\text{He}^{2+}$ of 100 keV/u. One observes that, after division of the data obtained with ${}^3\text{He}^{2+}$ by a constant factor (equal to 4), the low-energy wings of the two cusps could be superimposed within error limits. This was not possible at

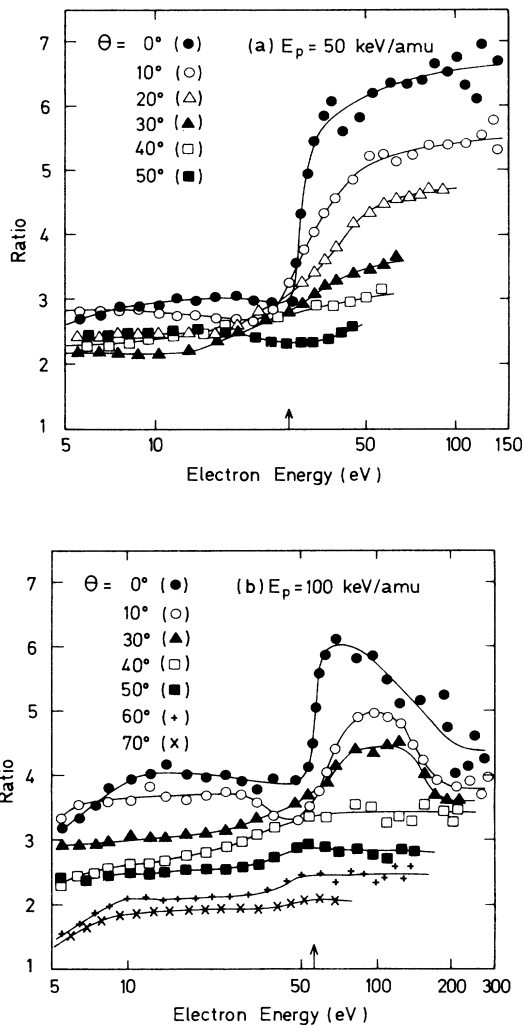


FIG. 7. Double differential ratio $R(E_e, \theta)$ of electron emissions induced by (a) 50-keV/u and (b) 100-keV/u ${}^3\text{He}^{2+}$ and H^+ projectiles interacting with He. The arrows indicate the ECC peak energy E_{eq} .

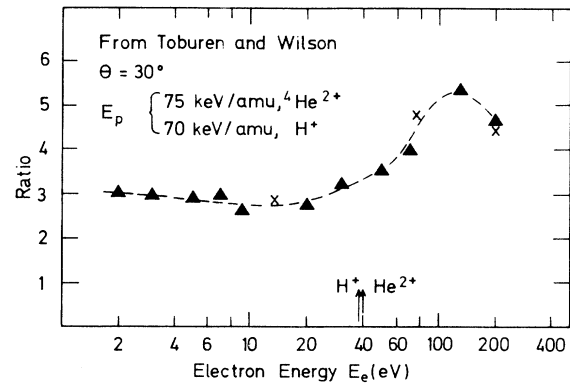


FIG. 8. Double differential ratio $R(E_e, \theta)$, as in Fig. 7 but for 75-keV/u ${}^4\text{He}^{2+}$ and 70-keV/u H^+ , extracted from DDCCS in (\blacktriangle) Fig. 1 and (\times) Fig. 5 of Toburen and Wilson (Ref. 31). The arrows indicate ECC peak energies E_{eq} .

energies $E_e \geq E_{\text{eq}}$. The high-energy wing of the ECC peak obtained with ${}^3\text{He}^{2+}$ stays clearly above that obtained with H^+ , giving rise to the step in R observed in Fig. 7(b).

The evidence from Fig. 9 permits an illuminating insight into the question of the dependence of convoy electron (ECC) yields on the projectile charge q . These yields have been defined as the integral of measured longitudinal ECC cusps ($\theta=0^\circ$) over a prefixed velocity interval, $v_p(1-0.04) \leq v_e \leq v_p(1+0.04)$,³³ and then compared with a dependence of the form q^n , as it resulted from theory.³⁴ Recent experimental determinations of such ECC yields by Kóvér *et al.*,³⁵ using H^+ and He^{2+} of energies between 400 and 700 keV/u, lead to a $q^{2.5}$ scaling, in reasonable agreement with a $q^{2.3}$ dependence, previously reported for heavier high-energy ions.³³ From the present measurements we obtain a $q^{2.2}$ dependence. It

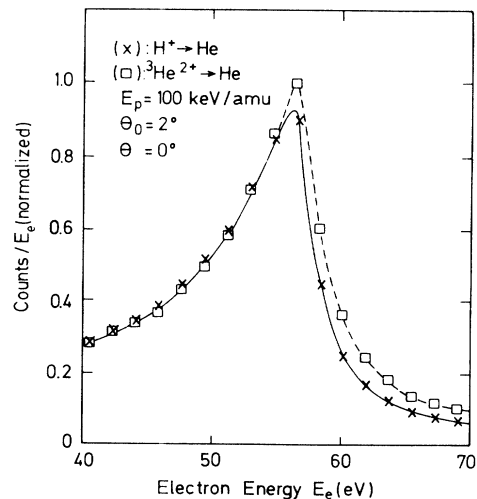


FIG. 9. ECC cusp taken with 100-keV/u ${}^3\text{He}^{2+}$ and H^+ respectively, normalized in such a way that they are superimposed in the low-energy wing by multiplying the H^+ data with 4.

must be noted that here, according to its definition, one deals with an integrated or average ECC yield. The theory of Dettmann³⁴ delivers a cusp which is scaled by a q^n power law (with $n=3$), and whose shape does not depend on the projectile charge q . Accordingly, a q^n power law would be valid also for what we may call a differential ECC yield. On the contrary, from Fig. 9 it is evident that the differential yield dependence on q is described by such a power law only in the low-energy wing of the cusp, where we find $n \approx 2$. Then the average yield dependence with $n \approx 2.2$ stems only from the much stronger enhancement of the differential yield for ${}^3\text{He}^{2+}$ found in the high-energy wing, that is, above E_{eq} . The conclusion is that a differential ECC yield dependence on the ionic charge q as seen in Figs. 7(a) and 7(b) cannot be accounted for by a description that considers only a one-center final-state interaction of the active electron.

A possible interpretation of the step in R , observed in E_{eq} , can be found by attributing it to a dependence of ECC cusp asymmetries on the projectile charge q . These asymmetries can be described in terms of the multipole expansion introduced in Refs. 8 and 36. Limiting our discussion to an expansion up to the second term only, we have, close to the ECC peak,

$$\frac{d\sigma}{d\mathbf{v}_e} = \frac{1}{v_e} \frac{d\sigma}{dE_e d\Omega} = \frac{1}{v'} (B_0^0 + B_1^0 \cos\theta'),$$

where v' is the electron velocity and θ' the emission angle, both defined in the moving projectile system. Since, during a collision, the relative influence of the attraction of the active electron by the residual target ion decreases with increasing q , the term B_1^0 , characterizing the diverging negative peak asymmetry, also decreases. Experimental evidence of this behavior has been formerly obtained by Andersen *et al.*,³⁷ they found, for 100 keV/u, $B_1^0/B_0^0 = -0.75$ for H^+ and $B_1^0/B_0^0 = -0.54$ for He^{2+} on He. Obviously such an interpretation is limited to a very close neighborhood of the ECC peak top.

It is, however, important to note that the increase of R extends itself almost up to the binary peak energy ($4E_{\text{eq}}$), and also up to angles where the ECC peak has totally disappeared. Therefore we compare our results with more general calculations based on the continuum-distorted-wave-eikonal-initial-state (CDW EIS) approximation. In Fig. 10 we show the ratio $R(E_e, \theta)$ as it results from the CDW EIS theory. A striking similarity with the experimental ratio $R(E_e, \theta)$ of Fig. 7(b) is observed. For electron energies $E_e < E_{\text{eq}}$ a decrease of R with increasing θ , that is, the enhanced ridge structure for the higher charge ${}^3\text{He}^{2+}$ ion is confirmed. Furthermore, we find an abrupt vertical step in R exactly at $E_e = E_{\text{eq}}$, where the ECC cross section diverges. In the experimental ratios of Fig. 7, the sharpness of this step can be considered as somewhat smeared out by the finite acceptance in energy and solid angle of the spectrometer.

Discrepancies remain, which may be attributed in part to the fact that the CDW EIS theory underestimates the DDCS at intermediate projectile energies and our measurements do not discriminate against processes which, besides single ionization, can contribute to the observed electron emissions. Coincidence measurements of Ander-

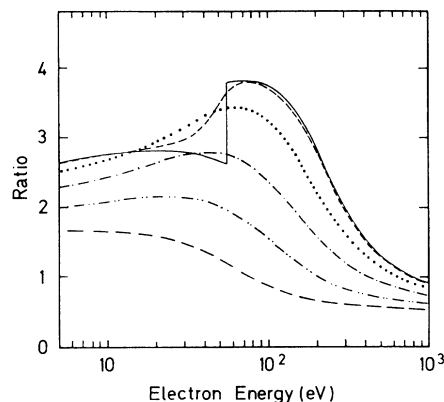


FIG. 10. CDW EIS calculation of the double differential ratio $R(E_e, \theta)$ of electron emissions induced by 100 keV/u ${}^3\text{He}^{2+}$ and H^+ projectiles interacting with He. (—), $\theta=0^\circ$; (---), $\theta=10^\circ$; (···), $\theta=30^\circ$; (-·-·-), $\theta=50^\circ$; (- - - -), $\theta=70^\circ$; (- - -), $\theta=90^\circ$.

sen *et al.*³⁸ suggest that, for 20-MeV Au^{q+} ($q=11$ and 15) on He, an enhancement of the high-energy tail of the ECC peak, similar to that observed in our Fig. 9, could be attributed to transfer ionization (TI). However, if we compare Figs. 7(a) and 7(b), we find that the step observed at 50 keV/u is conserved at 100 keV/u where, according to Table I, the contribution from TI is reduced from 32% to only about 10% of the total electron emission. Very recently, Kövér *et al.*³⁹ found that, for the case of 100-keV/u He^+ on He, a fraction of about 8% of the convoy electron yield is due to TI. Furthermore, one can expect from evidence in that work and Ref. 40 that, for the case of TI, the cusp width is strongly reduced on both cusp wings, compared to peak shapes obtained from ECC by bare ions.

IV. CONCLUSIONS

Our investigation of double differential electron emission, produced by bare ${}^3\text{He}^{2+}$ and H^+ ions of 50 and 100 keV/u, interacting with He under single-collision conditions, cover an ample range in electron energy E_e and angle θ . In regions of overlap they are in reasonable agreement with previous evidence. The ratio $R(E_e, \theta)$ of electron emission due to the doubly charged and singly charged projectiles shows two salient but substantially different deviations from the q^2 dependence predicted by first-order perturbative theories.

(i) At energies smaller than E_{eq} we obtain a decrease of this ratio with increasing emission angles, already found by Stolterfoht *et al.*¹⁶ and Platten and co-workers^{17,18} for the case of heavy projectiles of high energy. This means that the broad ridge, between the direct ionization and ECC peaks, which is attributed to two Coulomb center interaction of the active electron, is more pronounced for the projectile of higher charge. We interpret this results as a clear evidence for a dependence of saturation effects on the duration and intensity of the collisional interac-

tion; in other words, the relation between the kinetic projectile energy and the effective interaction potential.

(ii) For energies larger than E_{eq} , a sudden increase of $R(E_e, \theta)$ is observed. It accounts for a much stronger electron emission induced by the projectile of higher charge. This enhancement, which covers a broad range in energy and angle, leads us to the conclusion that, not only in the range between the direct ionization and ECC peaks, but also above the energy of the ECC peak, only a theory that considers the interaction with the two Coulomb centers can adequately describe the reported double differential electron emission ratios. We show that the CDW EIS ansatz of Rivarola and Fainstein¹⁹ furnishes a significant but not quantitative account of both these features.

Finally, we would like to remark that the evidence contained in our Fig. 7 has already been used in two recent papers by Reinhold and Olson⁴¹ for comparison with their classical trajectory Monte Carlo calculations. This method, which presents no restriction on the interaction of the electron with the projectile and residual target

ions, and includes all contributions to the differential electron emission, also renders a basic accordance with our experimental findings. In particular it describes the stepwise increase of $R(E_e, \theta)$ in the vicinity of the ECC peak top.

A maximum of the longitudinal electron emission, found recently by Olson *et al.*⁴² and Irby *et al.*⁴³ for energies between $E_e = 0$ and $E_e = E_{\text{eq}}$, and attributed to an enhanced emission of electrons "stranded" on the potential saddle between the projectile and residual target ions, is not confirmed, neither by our measured electron distributions nor by the CDW EIS calculations.

ACKNOWLEDGMENTS

We would like to thank J. E. Miraglia and C. O. Reinhold for useful discussion. One of us (W.M.) thanks J. Burgdörfer for helpful suggestions. We also are grateful to R. O. Barrachina for a critical reading of the manuscript. We would like to thank the Consejo Nacional de Investigaciones Científicas y Técnicas (Argentina) for financial support.

¹M. B. Shah and H. B. Gilbody, *J. Phys. B* **18**, 899 (1985), and references therein.

²H. Knudsen, *Invited Papers of the Twelfth International Conference on the Physics of Electronic and Atomic Collisions, Gatlinburg, 1982*, edited by S. Datz (North-Holland, Amsterdam, 1982), p. 657.

³G. H. Gillespie, *Phys. Lett.* **72A**, 329 (1979); *J. Phys. B* **15**, L729 (1982); *Phys. Lett.* **93A**, 327 (1983).

⁴J. E. Golden and J. H. McGuire, *J. Phys. B* **9**, L11 (1976).

⁵J. H. McGuire, A. Müller, B. Schuch, W. Groh, and E. Salzborn, *Phys. Rev. A* **35**, 2479 (1987).

⁶B. Brendlé, R. Gayet, J. P. Rozet, and K. Wohrer, *Phys. Rev. Lett.* **54**, 2007 (1985).

⁷G. C. Bernardi, S. Suárez, P. Focke, and W. Meckbach, *Nucl. Instrum. Methods* **B33**, 321 (1988).

⁸W. Meckbach, I. B. Nemirovsky, and C. R. Garibotti *Phys. Rev. A* **24**, 1793 (1981).

⁹A. Salin, *J. Phys. B* **2**, 631 (1969); J. Macek, *Phys. Rev. A* **1**, 235 (1970).

¹⁰D. R. Bates and G. W. Griffing, *Proc. Phys. Sec. London* **66**, 901 (1953).

¹¹V. H. Ponce and W. Meckbach, *Comments At. Mol. Phys.* **10**, 231 (1981).

¹²R. Shakeshaft and L. Spruch, *Phys. Rev. Lett.* **46**, 1571 (1981).

¹³W. Meckbach, P. R. Focke, A. R. Goñi, S. Suárez, J. Macek, and M. G. Menendez, *Phys. Rev. Lett.* **57**, 1587 (1986).

¹⁴G. C. Bernardi, S. Suárez, P. R. Focke, and W. Meckbach, in *Forward Electron Ejection in Ion Collisions*, Vol. 294 of *Lecture Notes in Physics* (Springer-Verlag, Berlin, 1987), pp. 286 and 295.

¹⁵C. R. Garibotti, D. Zanette, and M. L. Martiarena, in *Forward Electron Ejection in Ion Collisions*, Vol. 294 of *Lecture Notes in Physics* (Springer-Verlag, Berlin, 1987), p. 262.

¹⁶N. Stolterfoht, D. Schneider, J. Tanis, H. Altevogt, A. Salin, P. D. Fainstein, R. Rivarola, J. P. Grandin, J. N. Scheurer, S. Andriamonje, D. Bertault, and J. F. Chemin, *Europhys. Lett.* **4**, 899 (1987).

¹⁷H. Platten, G. Schiwietz, T. Schneider, D. Schneider, W.

Zeit, K. Musiol, T. Zouros, R. Kowallik, and N. Stolterfoht, *Proceedings of the Fifteenth International Conference on the Physics of Electronic and Atomic Collisions, Brighton, 1987*, edited by J. Geddes, H. B. Gilbody, A. E. Kingston, and C. J. Latimer (North-Holland, Amsterdam, 1987).

¹⁸P. D. Fainstein, V. H. Ponce, and R. D. Rivarola, *J. Phys. B* **21**, 287 (1988).

¹⁹R. D. Rivarola and P. D. Fainstein, *Nucl. Instrum. Methods* **B24/25**, 240 (1987).

²⁰G. C. Bernardi, P. D. Fainstein, C. R. Garibotti, and S. Suárez, *Proceedings of the International Conference on the Physics of Multiply Charged Ions, Grenoble, France, 1988*. [*J. Phys. (Paris)* **50**, C1-189 (1989)].

²¹J. S. Risley, *Rev. Sci. Instrum.* **43**, 95 (1972).

²²M. E. Rudd and D. H. Madison, *Phys. Rev. A* **14**, 128 (1976).

²³D. K. Gibson and I. D. Reid, *J. Phys. B* **19**, 3265 (1986).

²⁴M. E. Rudd, C. A. Sautter, and C. L. Bailey, *Phys. Rev.* **151**, 20 (1966).

²⁵M. E. Rudd and T. Jorgensen, *Phys. Rev.* **131**, 666 (1963).

²⁶M. E. Rudd, Y. K. Kim, D. H. Madison, and J. W. Gallagher, *Rev. Mod. Phys.* **57**, 965 (1985).

²⁷M. E. Rudd, L. H. Toburen, and N. Stolterfoht, *At. Data Nucl. Data Tables* **18**, 413 (1976); **23**, 405 (1979).

²⁸L. J. Puckett, G. O. Taylor, and D. W. Martin, *Phys. Rev.* **178**, 271 (1969).

²⁹C. O. Reinhold (private communication).

³⁰C. O. Reinhold, C. A. Falcón, and J. E. Miraglia, *J. Phys. B* **20**, 3737 (1987).

³¹L. H. Toburen and W. Wilson, *Phys. Rev. A* **19**, 2214 (1979).

³²H. Gabler, Ph.D. thesis, Freie Universität Berlin, 1974.

³³C. R. Vane, I. A. Sellin, M. Suter, G. Alton, S. B. Elston, P. M. Griffin, and R. S. Thoe, *Phys. Rev. Lett.* **40**, 1020 (1978).

³⁴K. Dettmann, K. G. Harrison, and M. W. Lucas, *J. Phys. B* **7**, 269 (1974).

³⁵A. Kövér, Gy Szabó, D. Berényi, L. Gulyas, I. Cserny, K. O. Groeneveld, D. Hofmann, P. Koschar, and M. Burkhard, *J. Phys. B* **19**, 1187 (1986).

³⁶C. R. Garibotti and J. E. Miraglia, *J. Phys. B* **14**, 863 (1981).

- ³⁷L. Andersen, K. E. Jensen, and H. Knudsen, *J. Phys. B* **19**, L161 (1986).
- ³⁸L. H. Andersen, M. Frost, P. Hvelplund, and H. Knudsen, *J. Phys. B* **17**, 4701 (1984).
- ³⁹Á. Kövér, L. Sarkadi, J. Pálinkás, D. Berényi, Gy Szabó, T. Vainai, O. Heil, K. O. Groeneveld, J. Gibbons, and I. A. Sel-
lin, *J. Phys. B* **22**, 1595 (1989).
- ⁴⁰L. Sarkadi, J. Pálinkás, Á. Kövér, D. Berényi, and T. Vainai,
Phys. Rev. Lett. **62**, 527 (1989).
- ⁴¹C. O. Reinhold and R. E. Olson, *J. Phys. B* **22**, L39 (1989);
Phys. Rev. A **39**, 3861 (1989).
- ⁴²R. E. Olson, T. J. Gay, H. G. Berry, E. B. Hale, and V. D.
Irby, *Phys. Rev. Lett.* **59**, 36 (1987).
- ⁴³V. D. Irby, T. J. Gay, J. Wm. Edwards, E. B. Hale, M. L.
McKenzie, and R. E. Olson, *Phys. Rev. A* **37**, 3612 (1988).